COBEM 2023 27TH INTERNATIONAL CONGRESS OF MECHANICAL ENGINEERING

ABCM Brazilian Society of Mechanical Sciences and Engineering
27th ABCM International Congress of Mechanical Engineering
December 04-08, 2023, Florianópolis-SC, Brazil

COB-2023-2378
COMPARATIVE PERFORMANCE ANALYSIS FOR DOUBLE-ROOF PYRAMID WAVEFRONT SENSOR

Tiago Giorgetti
Oswaldo Horikawa
Rodrigo Lima Stoeterau
Departamento de Engenharia Mecatrônica e Sistemas Mecânicos, Escola Politécnica da Universidade de São Paulo, Brazil
tgiorgetti@usp.br, ohorikaw@usp.br, rodrigo.stoeterau@usp.br

Alexandre T. S. Mello
Departamento de Eletrotécnica, Universidade Técnológica Federal do Paraná, Curitiba, Brazil
ajmello@professores.utfpr.edu.br

Abstract. *: Wavefront sensors a key optronic part in any modern telescope This work presents a performance study of the Double-Roof Pyramid wavefront sensor (DR-PWFS), consisting of two orthogonally positioned prisms, which offers some advantages over the Pyramid wavefront sensor (PWFS), one of the most significant being the reduced manufacturing cost. A study will be carried out in Zemax OpticStudio®, which performs simulations based on ray propagation, to verify the performance of the DR-PWFS sensor in comparison with the theoretical results obtained by Object-Oriented Matlab® Adaptive Optics (OOMAO) and to verifying the performance with the variation of some manufacturing parameters, such as "roof angle", thickness, distance between prisms and alignment variations. It is expected to establish parameters of any errors or aberrations associated with the use of these sensors, in particular the Double-Roof Pyramid and thus create a theoretical and practical support to assist in the development of prototypes on optical benches using DR-PWFS.*

Keywords: *adaptive optics, wavefront sensing, pyramid wavefront sensor*

1. INTRODUCTION

The occurrence of winds and convections induce turbulence in the atmosphere mixing layers with slightly different refractive indices, causes the amount of light entering the telescope's aperture change constantly, varying both the intensity and direction of the beam, and this phenomenon is known as seeing. There is a widely used way to characterize the seeing through a statistical parameter called "Fried parameter" $r0$. Seeing can be considered to indicate that an image can be degraded in two ways, through image movement and image blur. The larger the aperture of a telescope, the greater the degradation in the form of blur in the image, but it will suffer from less movement of the image over the field, while at small apertures the situation is opposite, suffering less from image blur, however, with the occurrence of greater movement of the image in the larger field (Bely et al., 2002).

Considering that in view of the need to obtain more and more sensitivity in the instruments from the increase in the diameter of the aperture of the telescopes, greater aperture, greater the degradation of the image, and to address this physical limitation, the use of Adaptive Optics – AO, is necessary and fundamental. This turns the systems capable of sensing and correcting an incident wavefront in real time (Hardy, 1998). The use of AO systems are being standard as new and larger telescopes are developed, and on the same path are the pyramidal wavefront sensors, as they offer greater sensitivity than the traditional Shack-Hartmann ones. As examples, the Thirty Mirror Telescope (TMT) (Veran et al., 2015), the Giant Magellan Telescope - GMT (Pinna, 2014) and the Extremely Large Telescope - ELT (Esposito, 2015) are all based on AO with an optical close loop using wavefront sensors.

The GMT is an aplanatic Gregorian telescope, different from the classic ones by its parabolic primary and a secondary mirror with a concave ellipsoid surface, which provide an improvement in quality from the image to an extensive field of view (GMT, 2018). The primary mirror is composed of 7 segments of 8.4 m in diameter each, the opening being equivalent effective gauge of 21.6 m in diameter. The secondary mirror is also segmented, works as a conjugate pair, and has a segment of 1.05 m in diameter working independently from its counterpart of the primary. Figure 1 shows two views of the telescope containing some dimensions and mass, and Figure 2 offers a view of primary and secondary mirrors arrangements for the GMT secondary.

.

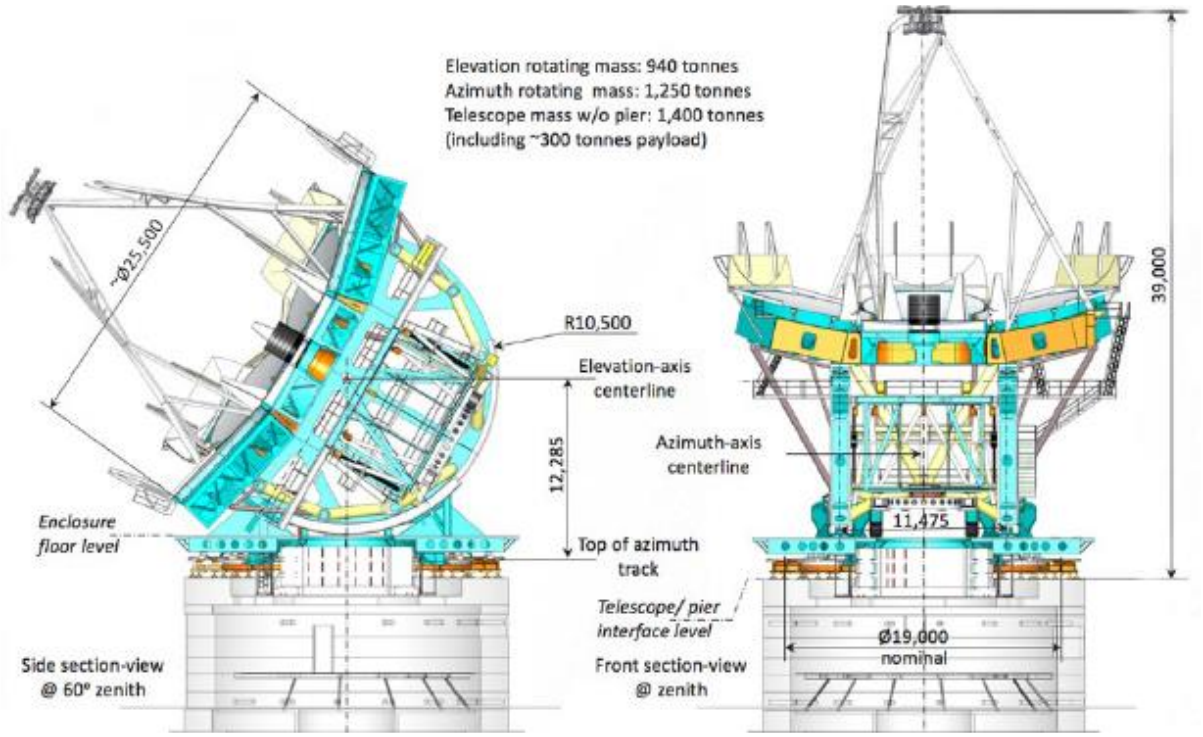

Figure 1. Views containing global dimensions of the telescope (GMT, 2018).

Although the Gregorian design is more compact, with a focal ratio of f/0.7, which offers some advantages over the traditional Cassegrain:

• The optically conjugated secondary mirror positioned approximately 165 m of the primary, allowing excellent correction by adaptive optics of the layer terrestrial over a large field of view, high performance, and low thermal background.

• Allows calibration for adaptive optics to be carried out by the telescope itself, with the production of an artificial star from the focus of the primary mirror (prime focus), which in this design is produced before the secondary surface.

• The focal plane of the telescope is curved towards the instrument (telecentric), simplifying the optics design for a wide-field, multi-object spectrograph 40 and diffraction limited, such as GMACS.

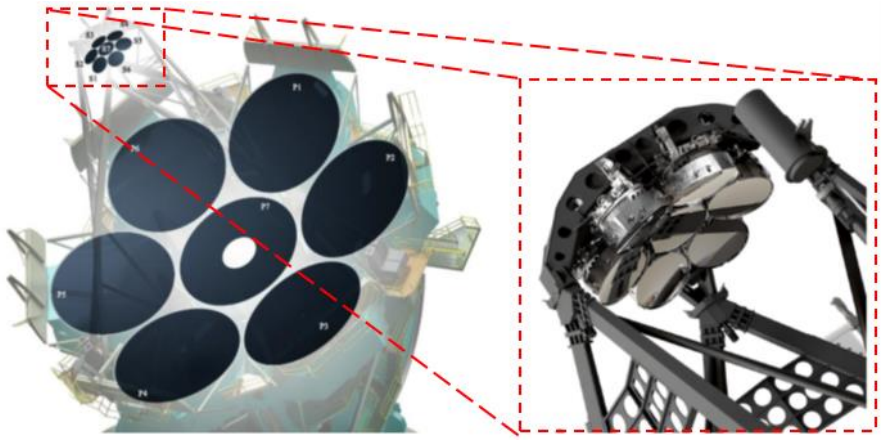

Figure 2. View of the primary and secondary mirror, both segmented and optically conjugated (Fanson et al., 2022).

The GMT can accommodate several instruments and the first generation was chosen to maximize scientific impact during early operations. Figure 3 shows cut-away view of the telescope that reveals the instrumentation stations below of the segments of the primary mirror, where the red, blue, and green rectangular boxes represent the volume available for instruments, such as Folded Ports - FP, Direct Gregorian - DG and the Gravity Invariant Station - GIS, and their respective locations accommodation. The yellow box indicates additional space for a fixed instrument called Instrument Platform - IP and all these ports allow them to be used by the least 10 instruments that can be simultaneously mounted and available for be operated (GMT, 2018).

1.1 Multi-Object Astronomical and Cosmological Spectrograph - GMACS

The GMT Multi-Object Astronomical and Cosmological Spectrograph (GMACS, GMT Multi-Object Astronomical and Cosmological Spectrograph), is one of the first light instruments and the first of the GMT Gregorian focus. Considered as one of the instruments that will be most used in the GMT, the GMACS is a critical instrument for the observatory.

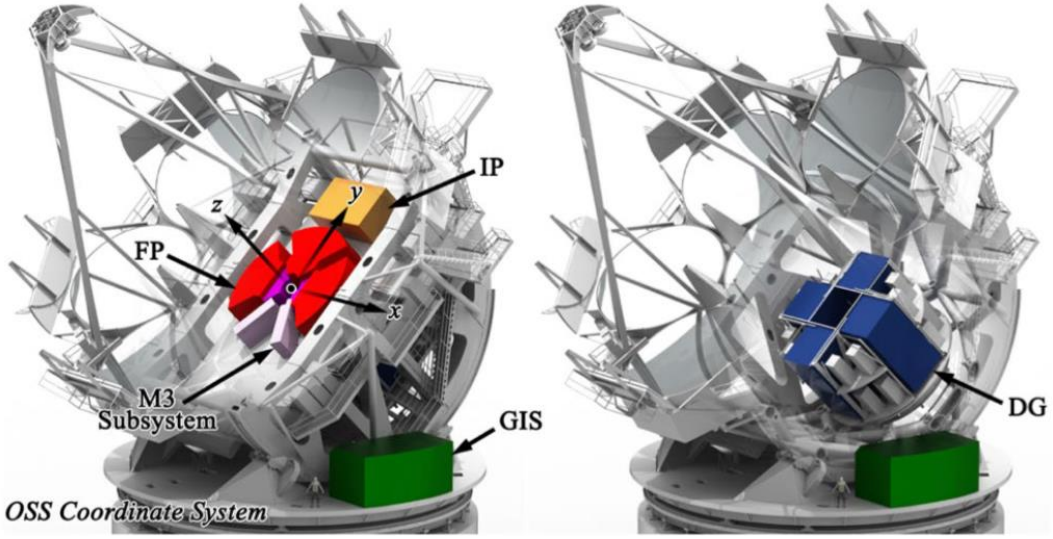

Figure 3. Sectional views of the GMT revealing the instrumentation ports. (GMT, 2018)

Due to its versatility, Ribeiro (2020) and Fanson et al. (2020) describe GMACS like a “workhorse”, as it is an instrument that performs imaging in a wide field of view, multi objects, with moderate resolution. The fact that it operates in the visible wavelength range of 0.32 μm to 1 μm, and have the ability to observe multiple targets simultaneously which is critical in the observation in areas like formation of stars, population of stars and more extragalactic sciences.

GMACS still houses, in its light entry window, the L3 lens of the Atmospheric Dispersion Corrector - ADC, this corrector changes the focal length of the telescope, offering a field of view of 20 minutes of arc, which ends up affecting the optical design of the wavefront sensors (GMTO, 2017).

1.2 On-Instrument Wavefront Sensor - OIWFS

The AGWS is an instrument installed on the top of the Gregorian Instrument Rotator – GIR and handles correct pointing errors generated by distortions in the wavefront caused by both due to atmospheric effects and distortions in the telescope to its location. Although distortions or mechanical deformations that occur. According to preliminary requirements the GMACS must provide the GMT Acquisition and Guiding wavefront system – AGWS with data image motion and global focus error at a minimum rate of 0.03 Hz, with the image motion measurements should be within a range of ±1.2 arcsec in natural mode seeing (GMTO, 2017).

1.2.1 The pyramid wavefront sensor

Proposed by Roberto Ragazzoni in 1996, he describes it as a compact wavefront sensor capable of generating four pupil images in a single detector, containing information on the gradient of an input wavefront (Ragazzoni, 1996). The sensor consists of a pyramidal prism, initially oscillating or modulated, usually circular, and contains a relay lens for beam collimation (Vérinaud, 2004). The apex of the pyramidal prism is positioned so that it is approximately in the nominal focal plane of the telescope objective.

The four faces of the prism cause a slight deflection towards the light in four different positions or quadrants. If there are negligible aberrations over a wide enough field of view, the relay lens can match the four apparent exit pupils into four images of pupils on the detector's surface. Care must be taken so that the angle of the pyramid's vertex is just a little less than 180° so that the images do not overlap (Ragazzoni, 1996).

Regarding the modulation of the vertex of the pyramidal prism, there is an increase in linearity and in the dynamic range of the detector. Ragazzoni, Diolaiti and Vernet (2002) present a study with the pyramidal sensor without modulation[8]. In addition to the advantage of providing an equivalent system without moving parts, it allows to ascertain the relationship between the modulation radius r and the diffusion angle σ, giving an equivalent answer for closed-loop systems as shown in equation (1).

$$\sigma = r\sqrt{\frac{\pi}{2}}, \quad (1)$$

To perform the averages of tip and tilt displacement, it is necessary to perform the centroid calculation evaluating the distribution of intensities I_1, I_2, I_3 and I_4 in the images of each pupil, for each pixel of corresponding position, according to the equations (2) and (3) (Vérinaud, C., 2004).

$$S_x(x,y) = \frac{[(I_1(x,y)+I_2(x,y))-(I_3(x,y)+I_4(x,y))]}{I_0}, \quad (2)$$

and

$$S_y(x,y) = \frac{[(I_1(x,y)+I_4(x,y))-(I_2(x,y)+I_3(x,y))]}{I_0}, \quad (3)$$

Where: $I_i(x, y)$ is the intensity at each sub-aperture located at (x, y) in quadrant i, integrated during the modulation cycle, and I_0 is the average intensity for each sub-aperture of the input beam.

1.2.2 The double-roof pyramid wavefront sensor

Imperfections in pyramidal prism fabrication and relay lenses can generate pupil mapping errors, impacting displacement measurements. Among them, the most common are error in the position of the center of the pupils, lateral color, differential distortion, and differential rotation. Some pyramidal prisms with extremely high angular tolerance of less than 5 arcsec, that produce an almost perfect pupils, corresponding to the detector pixel grid within ±0,2 pixel. In addition to difficulties and the associated costs to achieve these tight geometrical tolerances and find an appropriate manufacturing process (Lardière et al., 2019).

The fabrication of pyramidal prisms continues to be challenging because the vertex requires greater precision. The proposal then to solve this problem was the use of two identical roof-shaped prisms, positioned opposite each other and with the roof edge of one prism perpendicular to the other. Both roofs are positioned on the focal plane of the objective and must be in contact with a free spacing of $0.1\ mm$ in relation to each other. The Double-Roof Pyramid is optically equivalent to the single prism pyramidal sensor and contains some advantages such as:

1) The roof shape has a much lower production cost, so we expected these components to cost 70% to 98% more than equivalent DR prims;

2) No need to worry about the fabrication of the vertex; and

3) The edges between the two surfaces forming the roof can be sharpened to a tolerance of approximately $5\,\mu m$ without great effort.

One downside about the Double-Roof Pyramid sensor is that it has more surfaces along the optical axis compared to the single pyramidal prism, which impacts sensor performance. Mounting and aligning the prisms is not a difficult task if mechanical supports with proper tolerance are used. The use of a spacer will prevent the prisms from colliding and will keep the suggested spacing of $0.1\ mm$ or as little as possible. Collisions of any intensity must be avoided as they will damage both edges of the roof (Lardière et al., 2019).

1.4 Work Delimitation

This work presents an optical performance study of the Double-Roof Pyramid Wavefront Sensor - DR-PWFS, consisting of two orthogonally positioned prisms, which offers a few advantages over the Pyramid Wavefront Sensor - PWFS. One of the most significant is the reduced manufacturing cost (Lardière et al., 2019). Figure 4 shows PWFS, BK7 glass with imensions $25\ x\ 25\ x\ 10\ mm$ and a 30-degree vertex angle.

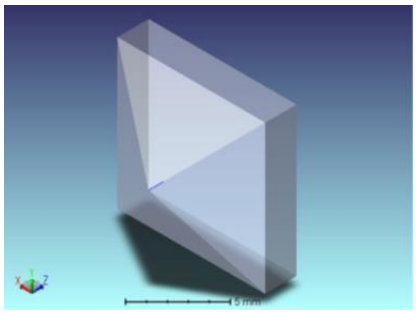

Figure 4. The one prism pyramid wavefront sensor modeled and used in the simulation.

Sharp edges of less than 5μm are usually manufacturable for DR prisms. However, this requirement presents a significant challenge in polishing the four faces and meeting with one apex in 5μm for Pyramid prisms. To compare with an equivalent sensor. Figure 5 shows DR-PWFS used in pair, to mimic the one prism Pyramid effect of conjugate the four pupil images. The dimensions were the same of PWFS 25 x 25 x 10 mm, BK7 glass for each prism and 30-degree for the roof angle. For this mount, the nominal focal plane of the telescope objective must be between the prisms, where there is an air gap of 0.1 mm or less, avoiding having contact with the prisms, and one is mounted 90-degree in the z-axis.

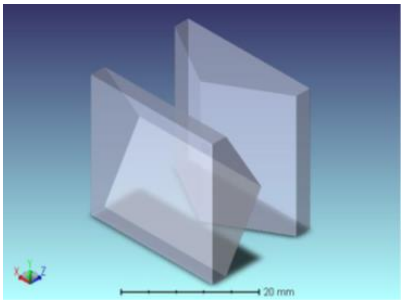

Figure 5. Double roof pyramid prisms positioned at optic axis with 0.1 mm air gap between and one tilted 90-degree in z-axis.

2. MODELING

The modeling and analysis were performed using Zemax OpticStudio® 22.1 Software. To mimic the effect of a modulation, the fields were configured for a single central and four peripheral fields of 0.1 degrees box size, just so that the rays could reach both the face of the roof planes and the four pyramid faces when modulation is required to blur the image at apex position6. For the design in Figure 6, the pyramid prism apex is positioned at the telescope focal plane, and a relay lens images the entrance pupil.

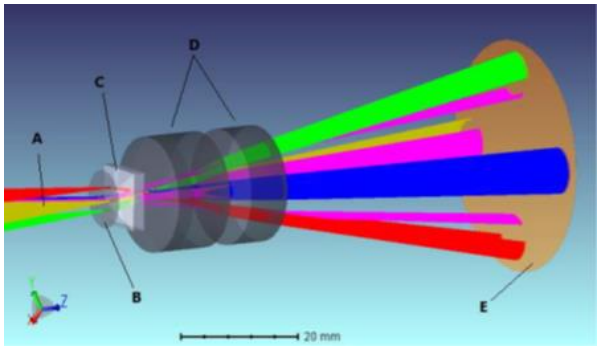

Figure 6. Pyramid optical design. In (A) the $f/4.5$ beam with one central field and four peripheral fields 0.05 degrees quadrant separation, (B) the nominal focal plane of telescope objective where the vertex of pyramid prism is positioned, (C) the PWFS, (D) the relay lens and (E) the detector surface when the pupil imagens will be conjugated.

Figure 7 has a double-roof pyramid arrangement with a 0.1 mm air gap between them, with the telescope focal plane in the middle of the prisms. A barlow lens was installed before the prisms to decrease the speed, offering an $f/17$ optics. Following the prisms, a relay lens images the entrance pupil (LOZI et al., 2019).

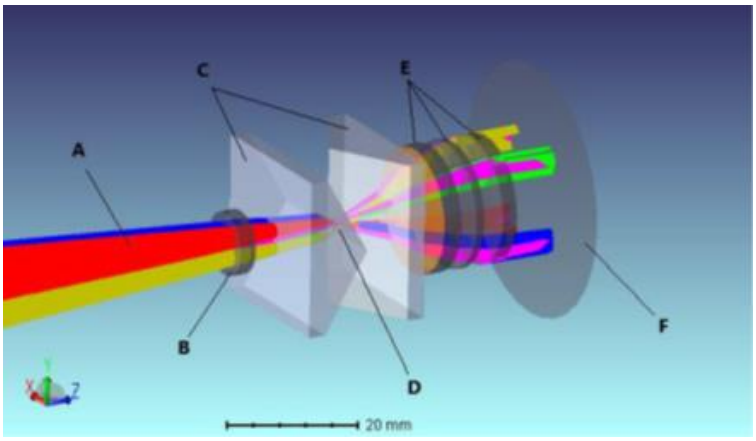

Figure 7. Double-roof pyramid optical design. In (A) the telescope beam with one central field and four peripheral quadrant fields, (B) a negative lens (barlow) to decrease the speed for $f/17$ optics, (C) the double-roof prisms positioned 0.1 mm (roof distance) of air gap, place of telescope focal plane (D), the relay lens (E) and (F) the detector surface when the four pupil images will be conjugated.

3. RESULTS

The entrance pupil imaging results for the optical pyramid design show considerably less lateral distortion than that found in the double roof optical design. The reason is because of the prism itself, with greater influence on the roof prism. Figure 8 shows the detector surface image of incoming vertex pyramid central field beam that simulate no-modulation of the sensor. With an image width of 42 mm and a field size of 0.07 degrees is possible to see a small lateral distortion and an energy efficiency of 65.7%.

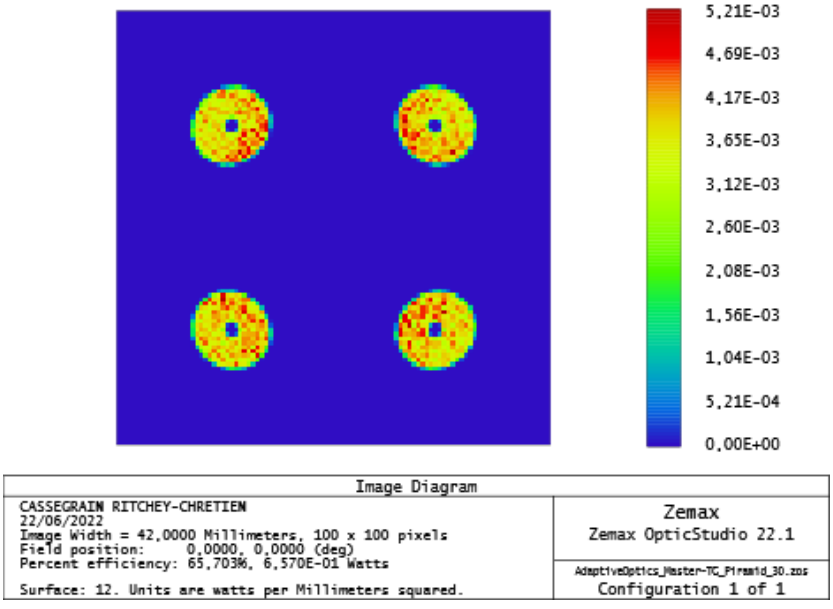

Figure 8. Results for PWFS in a paraxial field.

As shown in Figure 9, each peripheral field is positioned in the relative quadrant figure position. In this case the four fields mimic a modulated prism that have a radius of 0.05 degrees from paraxial field where there is an increase in dynamic range. Also is possible to notice a presence of a small lateral distortion.

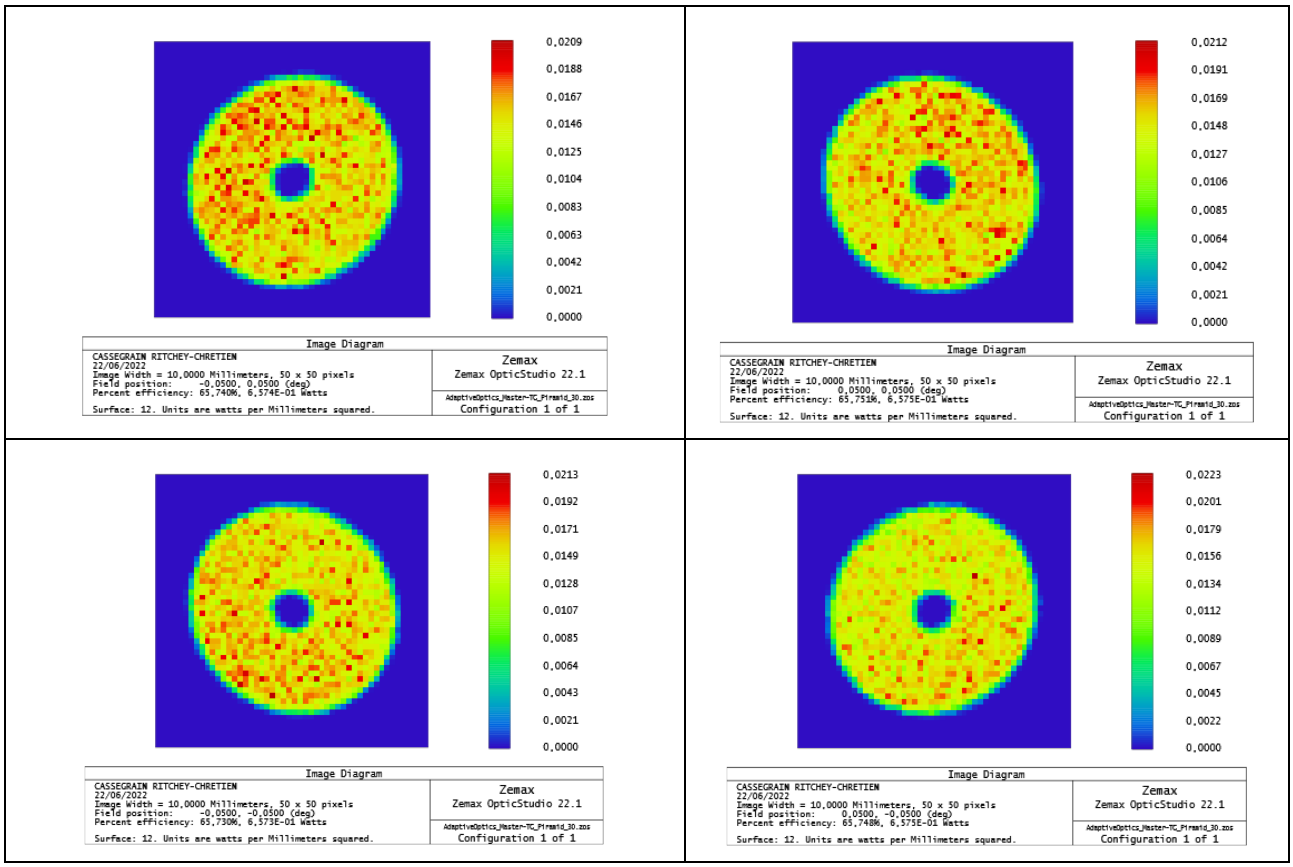

Figure 9. Results for PWFS in a peripheral field.

An important lateral distortion is noticed in Figure 10, where a 20 *mm* image width and a filed size of 0.1 degree from detector surface is conjugated from a telescope paraxial field. This case mimics a no-modulation prism effect, resulting in an energy efficiency of 94%.

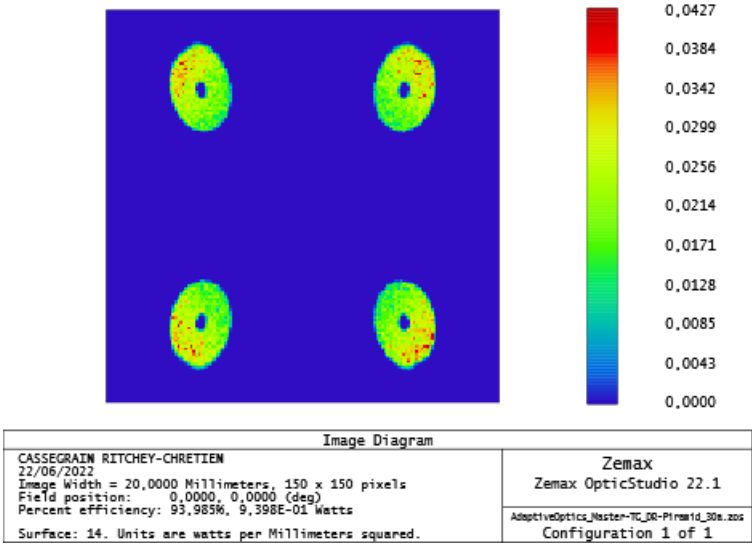

Figure 10. Results for DR-PWFS in a paraxial field.

In Figure 11, each peripheral field is positioned in the relative quadrant figure position. In this case the four fields mimic a modulated prism that have a radius of 0.05 degrees from paraxial field where there is an increase in dynamic range. Also is possible to notice a presence of an important lateral distortion.

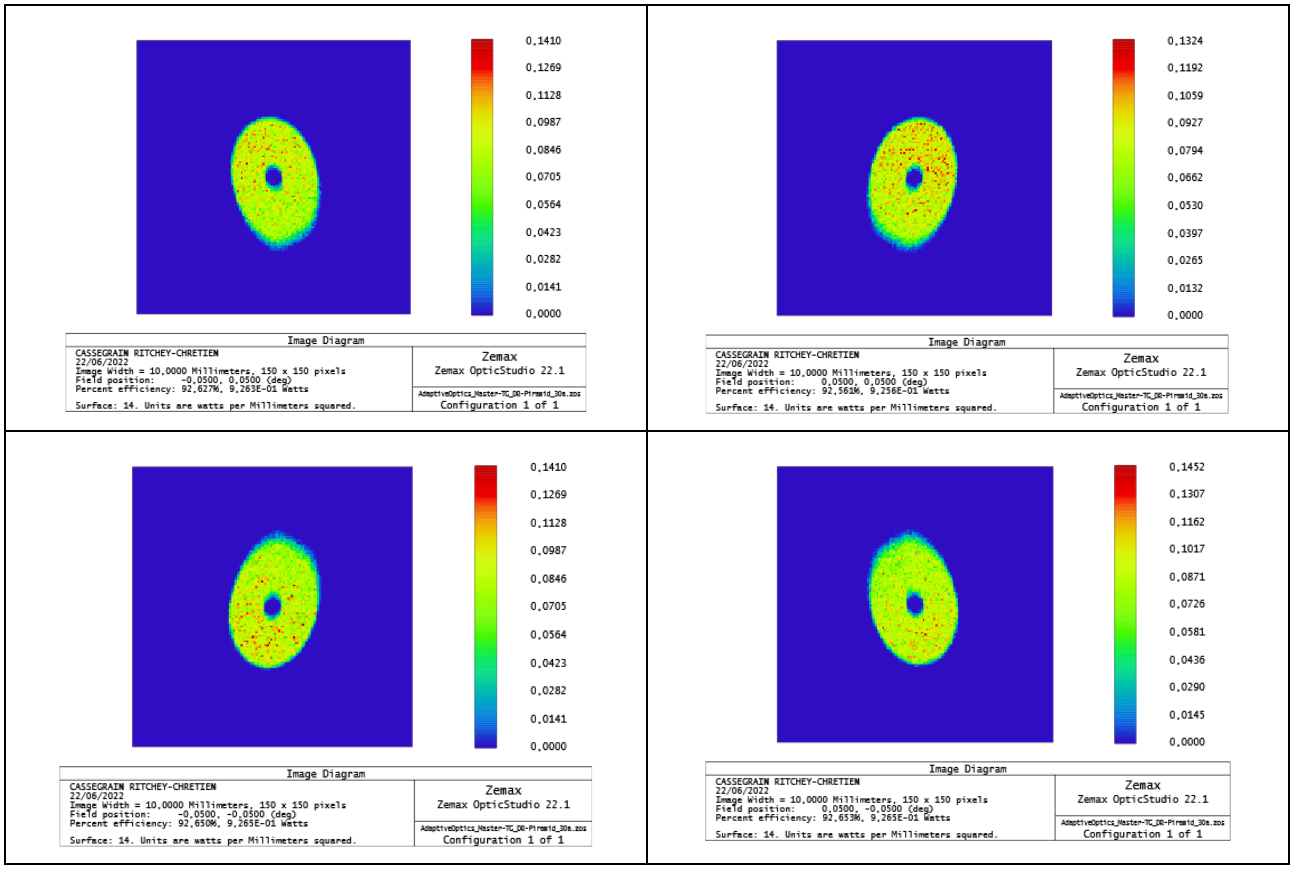

Figure 11. Results for DR-PWFS in a peripheral field.

4. CONCLUSION

The results of the simulation evaluated the limitations of the double-roof pyramid WFS, as well as its loss in precision, so that the design of prisms and optical support elements can be improved. The importance of pyramidal vertex angle show that is direct related to the lateral distortion as well the combination with f-number. For the next step, in optical bench test assembly, tests will be performed to meet theoretical limitations with the experimental ones.

REFERENCES

Bely, P. et al., 2002. Design and construction of large optical telescopes, 505 p. ISBN 0387955127.

Hardy, J. W., 1998. Adaptive optics for astronomical telescopes. New York: Oxford series in optical and imaging science. ISBN 0-19-509019-5.

Veran, J., Esposito, S., Spano, P., Herriot, G., & Andersen, D., 2015. Pyramid versus Shack-Hartmann: Trade Study Results for the NFIRAOS NGS WFS. Adaptive Optics for Extremely Large Telescopes 4 – Conference Proceedings, In: http://dx.doi.org/10.20353/K3T4CP1131568

Pinna, E., 2014. Design and numerical simulations of the GMT Natural Guide star WFS, Adaptive Optics Systems IV, 2014, vol. 9148. doi:10.1117/12.2057059.

Esposito, S., 2015. NGS WFSs module for MAORY at E-ELT, Memorie della Societa Astronomica Italiana, vol. 86, p. 446, 2015.

Ragazzoni, R., 1996. Pupil plane wavefront sensing with an oscillating prism. Journal of Modern Optics, v. 43, n. 2, p. 289-293.

Vérinaud, C., 2004. On the nature of the measurements provided by a pyramid wave-front sensor. Optics Communications, v. 233, n. 1-3, p. 27-38.

Ragazzoni, R.; Diolaiti, E.; Vernet, E., 2002. A pyramid wavefront sensor with no dynamic modulation. Optics Communications, v. 208, n. 1-3, p. 51-60.

Lardière, O. et al., 2017. Double-pyramid wavefront sensors: Tolerance relaxation and cheaper alternatives using achromatic double-roof prisms. Adaptive Optics for Extremely Large Telescopes, AO4ELT5, v. 2017-June, n. May 2018, p. 1-9.

Lozi, J. et al., 2019. Visible and near-infrared laboratory demonstration of a simplified pyramid wavefront sensor. In: Publications of the Astronomical Society of the Pacific, IOP Publishing, v. 131, n. 998, p. 044503.
GMT Science Book, 2018. Giant Mallegan Telescope Science Book 2018. GMTO Corporation, 2018. In: https://giantmagellan.org/wp-content/uploads/2018/11/
GMT Science Book, 2021. Giant Mallegan Telescope Science Book 2021. GMTO Corporation, 2021. In: https://giantmagellan.org/wp-content/uploads/2021/11/
GMTO Corporation. GMT-DOC-01369 - Wavefront Control Architecture, 2017.
GMTO Corporation. GMT-DOC-00010-rev.H GMT Optical Design, 2019.

RESPONSIBILITY NOTICE

The authors are the only responsible for the printed material included in this paper.